Journal of Power Sources 183 (2008) 454–463

Contents lists available at ScienceDirect

Journal of Power Sources

journal homepage: www.elsevier.com/locate/jpowsour

Zeolite beta-filled chitosan membrane with low methanol permeability for direct methanol fuel cell

Yabo Wang, Dong Yang, Xiaohong Zheng, Zhongyi Jiang*, Jie Li

Key Laboratory for Green Chemical Technology, School of Chemical Engineering and Technology, Tianjin University, Tianjin 300072, China

ARTICLE INFO

Article history:
Received 24 April 2008
Received in revised form 3 June 2008
Accepted 4 June 2008
Available online 8 June 2008

Keywords:
Direct methanol fuel cell
Methanol permeability
Hybrid membrane
Zeolite beta
Chitosan

ABSTRACT

Zeolite beta particles with different sizes and narrow size distribution were hydrothermally synthesized and incorporated into chitosan (CS) matrix to prepare CS/zeolite beta hybrid membranes for direct methanol fuel cell (DMFC). It was found that the chitosan membrane filled by zeolite beta particles about 800 nm in size exhibited the lowest methanol permeability, which can be ascribed to their optimum free volume and methanol diffusion characteristics. To further improve the performances of CS/zeolite beta hybrid membranes, zeolite beta particles about 800 nm in size were sulfonated via three different approaches. The results indicated that the introduction of sulfonic groups could reduce the methanol permeability further as a result of the enhanced interfacial interaction between zeolite beta and chitosan matrix. Furthermore, in terms of the overall selectivity index, CS/zeolite beta hybrid membranes were comparable to Nafion® 117 membrane at low methanol concentration (2 mol L^{-1}) and much better at high methanol concentration (12 mol L^{-1}).

1. Introduction

Organic/inorganic hybrid membrane has attracted much attention as proton exchange membrane (PEM) for direct methanol fuel cell (DMFC) in recent years. It has been demonstrated that the inorganic moiety in the organic/inorganic hybrid membrane plays an important role in methanol rejection since it can build up a physical barrier against the methanol crossover [1], tune the microstructure and hydrophilic–hydrophobic balance of the hybrid membrane [2,3]. Meanwhile, in most cases, the presence of inorganic moiety can significantly enhance the thermal and mechanical stability of the hybrid membrane [4,5]. Till now, many kinds of inorganic fillers, such as silica, titanium oxide, zirconium oxide, aluminum oxide, montmorillonite, heteropolyacid and zeolites [6–15], have been employed to develop organic/inorganic hybrid membranes for DMFC application.

Recently, many efforts have been devoted to the organic/inorganic hybrid membranes using zeolite as inorganic filler, owing to its high stability, facile modification and well-defined microporous structure. The Nafion® membranes filled with different kinds of zeolite particles have been demonstrated to possess low methanol crossover and high proton conductivity [16–18]; however, the high cost of Nafion® membrane severely limits its wide application. In our previous studies [19–21], chitosan (CS) membranes filled by commercially purchased mordenite, A, X, Y, and ZSM-5 zeolite were prepared, which showed a remarkable decrease in methanol crossover compared with Nafion® 117 membrane. During the preparation of CS/zeolite hybrid membranes, the ball-milling method was often utilized to reduce the size of zeolite particles. Nevertheless, the resultant zeolite particles often exhibited still large size (micrometer scale), wide size distribution, and irregular shape, leading to the frequent generation of many non-selective voids at the interface of zeolite and chitosan matrix. This can substantially increase the free volume cave size of the membrane [19,22] and methanol diffusion rate in CS/zeolite hybrid membrane correspondingly.

In this study, zeolite beta particles with different sizes were hydrothermally synthesized, and then incorporated into chitosan matrix to prepare CS/zeolite beta hybrid membranes. Zeolite beta was chosen as inorganic filler, because its hydrophobic nature may ensure its low methanol crossover [21], and its moderate surface acidity [23] can enhance its bonding with chitosan matrix. Taking low methanol permeability, relatively high proton conductivity, environmental benignity and low cost into account, chitosan was chosen as the bulk polymer [24–26]. Hopefully, a kind of CS/zeolite beta hybrid PEM with low methanol permeability for DMFC application can be acquired through rationally controlling the morphology, size distribution, and surface properties of zeolite beta particles.

* Corresponding author. Tel.: +86 22 27892143; fax: +86 22 27892143.
E-mail address: zhyjiang@tju.edu.cn (Z. Jiang).

0378-7753/$ – see front matter © 2008 Elsevier B.V. All rights reserved.
doi:10.1016/j.jpowsour.2008.06.003

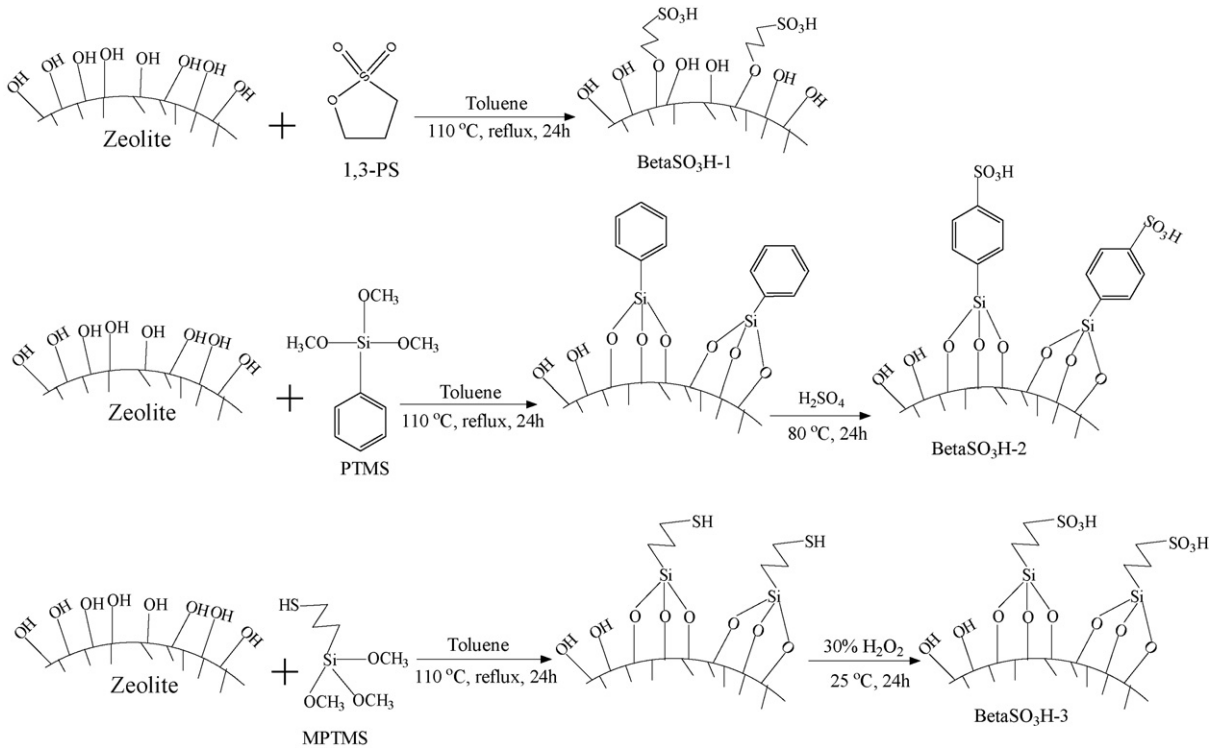

Scheme 1. Schematic representation of sulfonation processes of zeolite beta.

2. Experimental

2.1. Materials and chemicals

Fumed silica (Degussa, Aerosil 200) was purchased from Shanghai Haiyi Scientific & Trading Co., Ltd. 3-mercaptopropyltrimethoxysilane (MPTMS, 98 wt.%) and phenyltrimethoxysilane (PTMS, 94 wt.%) were supplied by Dow Corning (Shanghai) Co., Ltd. 1, 3-propane sultone (1, 3-PS, 99 wt.%) was purchased from Wuhan Bright Chemical Co., Ltd. Chitosan with a deacetylation degree of 90% was supplied by Zhejiang Golden-shell biochemical Co., Ltd. Tetraethylammonium hydroxide (TEAOH, 25 wt.% aqueous solution), aluminum powder, ammonium fluoride, acetic acid, sulfuric acid and methanol were of analytical grade and purchased locally. De-ionized water was used in all experiments.

2.2. Synthesis and sulfonation of zeolite beta

Zeolite beta particles were synthesized according to the procedure described in the literatures [27,28]. In a typical process, the initial precursor gel had the molar composition of $10TEAOH:25SiO_2:Al:375H_2O$. The aluminum powders were dissolved in one portion of TEAOH aqueous solution to form a clear solution, and then mixed with the slurry containing fumed silica and the other portion of TEAOH aqueous solution. The formed aluminosilicate fluid gel was stirred at room temperature for 4 h, and then transferred into a 100 mL Teflon-lined stainless steel autoclave. The crystallization was carried out at 140 °C, either under the rotational state in an oil bath for 2 days or under the static state in an oven for 3 days. After crystallization, the autoclaves were quenched in cold water to terminate the synthesis procedure. The product was separated by centrifugation, washed with de-ionized water until pH <9.0 and then dried at 60 °C for 24 h. Thereafter, the calcination procedure (550 °C, 12 h) was introduced to remove the template agent and obtain hydrogen-type zeolite beta. For simplicity, zeolite beta particles synthesized under rotational and static state were denoted as Beta-1 and Beta-2, respectively. In order to obtain zeolite beta with relatively large size, a certain amount of NH_4F with the molar ratio of $Al:20NH_4F$ was added into the above precursor. Then, the crystallization was carried out under static state in an oven at 140 °C for 10 days. The resultant zeolite beta was denoted as Beta-3.

As illustrated in Scheme 1, the sulfonation of Beta-2 sample was performed using the surface hydroxyl groups of zeolite beta by dehydration with 1, 3-PS or condensation with PTMS and MPTMS as sulfonic acid precursors. The reactions were carried out at the refluxing temperature of toluene (110 °C) for 24 h with the molar ratio of Beta-2 sample, sulfonic acid precursor and toluene of 1:2:20. Sultone precursor (1, 3-PS) directly endowed the sulfonic acid groups from ring opening of sultone and did not need further treatment after the surface functionalization of zeolite beta. In the case of phenyl group precursor (PTMS), the phenyl groups grafted onto zeolite beta further reacted with concentrated sulfuric acid at 80 °C for 24 h. As for thiol precursor (MPTMS), the mercapto groups grafted onto zeolite beta was oxidized into sulfonic acid groups with 30 wt.% H_2O_2 solution at 25 °C for 24 h. The prepared samples were filtered and washed with ethanol and water to remove the precursor residues. Functionalized samples were dried and denoted as $BetaSO_3H$-1, $BetaSO_3H$-2 and $BetaSO_3H$-3, where 1, 2, 3 represented the sulfonic acid precursor of 1, 3-PS, PTMS and MPTMS, respectively.

2.3. Membrane preparation

75 g 2.0 wt.% aqueous solution of acetic acid was equally divided into two portions. 1.5 g CS powders were dissolved in one portion of acetic acid solution at 80 °C. A certain amount of zeolite beta was dispersed in the other portion of acetic acid solution by ultrasonic treatment for 30 min. Subsequently, two portions of solution were mixed, and stirred at 80 °C for 30 min. Then, ultrasonic treatment

and stirring were carried out alternatively, each for 30 min. After thorough degasification, the mixture was cast onto a clean glass plate and dried at room temperature for 48 h. Next, the membrane was immersed in 2 mol L^{-1} H_2SO_4 for 24 h to allow cross-linking. Thereafter, the membrane was repeatedly rinsed with de-ionized water to remove residual H_2SO_4, and dried in vacuum at 25 °C for 24 h. Finally, the CS/zeolite beta hybrid membrane was obtained. Pure CS membrane was prepared in the same way in the absence of zeolite beta particles.

The CS membranes filled by zeolite beta particles were designated as CS/Beta-*a*-*b*, where Beta-*a* (*a* = 1, 2, or 3) represented the zeolite beta samples prepared under different conditions, and *b* (10–50%) represented the weight ratio of zeolite beta to CS. The CS membranes filled by sulfonated zeolite beta particles were designated as CS/BetaSO_3H-*c*-*d*, where BetaSO_3H-*c* (*c* = 1, 2, or 3) represented the zeolite beta samples sulfonated by different precursors, and *d* (10–50%) represented the weight ratio of sulfonated zeolite beta to CS.

2.4. Characterizations

The morphology of zeolite beta and membranes was observed with transmission electron microscopy (TEM, JEM-100CX II) and scanning electron microscopy (SEM, Philips XL30ESEM). The crystalline structure of zeolite beta and membranes was investigated with an X-ray diffractometer (RigakuD/max2500v/pa, Cu Kα, 40 kV, 200 mA, 8° min^{-1}) in the range of 5°–50°. Thermogravimetric analysis (TGA) was carried out on a PerkinElmer TG/DTA thermogravimetric analyzer at a heating rate of 10 °C min^{-1} under air flow of 30 mL min^{-1} from room temperature to 800 °C. Fourier transform infrared (FT-IR) spectra of zeolite beta samples and membranes were recorded using a Nicolet-740, PerkinElmer-283B FT-IR Spectrometer with a resolution of 4 cm^{-1}. The chemical state of sulfur element on the surface of sulfonated zeolite beta was characterized by using X-ray photoelectron spectroscopy (XPS, PerkinElmer PHI 1600 Mg Kα radiation for excitation), and the relative content of sulfur was calculated by the ratio of sulfur content to aluminum content.

2.5. Water and methanol uptake

The water and methanol uptake of membrane were determined by measuring the weight difference of membrane before and after immersion in water or an aqueous solution of methanol. Membrane samples dried under vacuum at 25 °C for 24 h were weighted (W_{dry}), and then immersed in water or 12 mol L^{-1} aqueous solution of methanol at room temperature for 24 h. After wiped with a filter paper to remove the residual water or methanol solution on the surface of membrane, the wet membrane was weighted (W_{wet}). The water or methanol uptake was calculated according to Eq. (1). Three parallel experiments were conducted and the experiment error was within ±5.0%.

$$\text{Uptake}\,(\%) = \frac{W_{wet} - W_{dry}}{W_{dry}} \times 100 \quad (1)$$

2.6. Ion exchange capability (IEC)

The IEC of membrane was determined by a titration method. A pre-weighted membrane was immersed in NaCl solution of 2 mol L^{-1} for 24 h to replace H^+ by using Na^+ completely. The remaining solution was then titrated with a 0.01 mol L^{-1} NaOH solution using phenolphthalein as an indicator. The IEC (mmol g^{-1}) was calculated by Eq. (2), where V_{NaOH} (L) is the volume of NaOH solution consumed in the titration and W_d (g) is the weight of dry membrane.

$$\text{IEC} = \frac{0.01 \times 1000 \times V_{NaOH}}{W_d} \quad (2)$$

2.7. Methanol permeability

The methanol permeability was measured with a glass diffusion cell as described in the literature [19], which consists of two compartments with identical volume separated by the membrane sheet. Before fixed on the diffusion cell, the membrane was prehydrated in de-ionized water for 24 h. The measurement started when the de-ionized water and methanol solution (2 or 12 mol L^{-1}) were filled in two compartments, respectively. The methanol concentration in the water compartment was determined using a gas chromatography (Agilent 6820) equipped with a TCD detector and a DB624 column. The methanol permeability (*P*, cm^2 s^{-1}) was calculated by Eq. (3),

$$P = \frac{SV_B L}{AC_{A0}} \quad (3)$$

where *S* is the slope of curve of methanol concentration versus time in the water compartment; V_B (mL) is the volume of water compartment; C_{A0} (mol L^{-1}) is the initial concentration of methanol in the methanol compartment; *L* (cm) and *A* (cm^2) are the thickness and area of the membrane, respectively. Each sample was measured three times and the average value of *P* was calculated with an error within ±6.5%.

2.8. Proton conductivity

The proton conductivity of membrane in the transverse direction was measured in two-point-probe conductivity cells with a frequency response analyzer (FRA, Autolab PGSTST20) by the AC impedance spectroscopy method. Prior to measurement, the membrane sample was equilibrated in 0.2 mol L^{-1} H_2SO_4 for 24 h. The measurement was performed in a frequency range of 1–10^6 Hz with oscillating voltage of 10 mV at room temperature (20 ± 1 °C). The proton conductivity (σ, S cm^{-1}) of membrane was calculated by Eq. (4),

$$\sigma = \frac{L}{AR} \quad (4)$$

where *L* (cm) and *A* (cm^2) are the thickness and testing area of the membrane sample, respectively, and *R* is the membrane resistance derived from the low intersection of the high frequency semicircle on a complex impedance plane with Re (*z*) axis.

3. Results and discussion

3.1. CS/Beta hybrid membrane

3.1.1. Morphology and structure of zeolite beta

The morphology of zeolite samples was observed by SEM and TEM. As shown in Fig. 1, both Beta-1 (Fig. 1a) and Beta-2 (Fig. 1b) samples appeared round shape with the diameters about 300 and 800 nm, respectively; while Beta-3 sample (Fig. 1c) exhibited irregular shape about 5 μm in size. The XRD spectra of zeolite samples were conducted to determine their crystalline structure. From Fig. 2, it can be observed that all the zeolite samples exhibited two intense peaks located at 7.7° and 22.6°, indicating that zeolite beta was the main crystalline form in the samples [27,28].

3.1.2. Structure of CS/Beta hybrid membranes

Fig. 3 showed typical cross-section SEM images of CS and CS/Beta hybrid membranes. All the membranes had the thickness

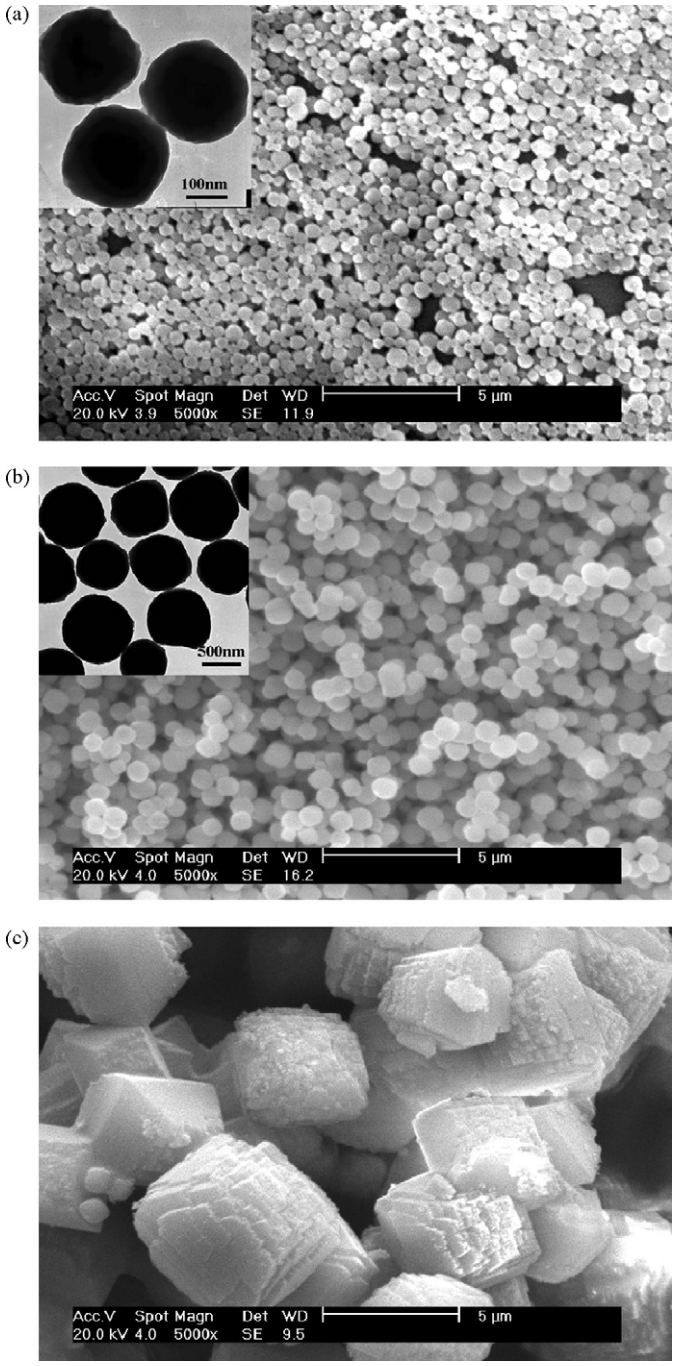

Fig. 1. SEM and TEM (inset) images of zeolite beta samples: (a) Beta-1; (b) Beta-2 and (c) Beta-3.

of 35–45 μm. No obvious agglomeration of zeolite beta particles was observed in CS/Beta-1–30% and CS/Beta-2–30%, indicating that zeolite beta particles with diameter of 300–800 nm can be well dispersed in CS matrix (Fig. 3b and c). However, the sedimentation of zeolite beta particles occurred in CS/Beta-3–30% (Fig. 3d), since the size of Beta-3 (5 μm) was too large. This led to the formation of separated zeolite beta and chitosan layers in hybrid membrane, just as a composite membrane constituting inorganic and organic layers.

The XRD spectra of CS and CS/Beta-2 hybrid membranes were presented in Fig. 4. Pure CS membrane showed four characteristic peaks of chitosan at 11.6°, 18.5°, 23.7° and 26.5°, which was similar to that reported in the literature [29]. The broad peak at around

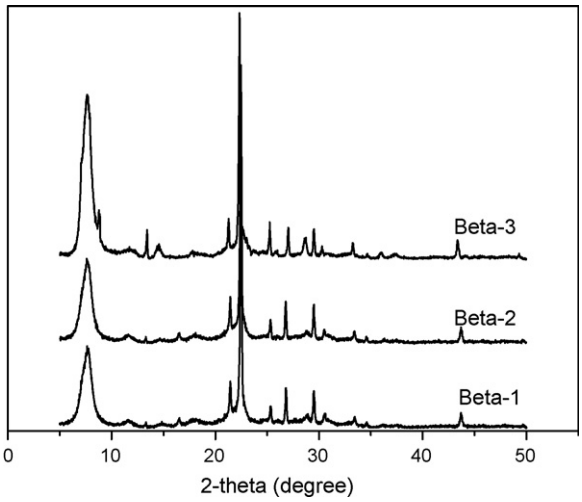

Fig. 2. XRD spectra of zeolite beta samples.

20° was attributed to the partly crystallized chitosan chains. It was noted that the intensity of chitosan characteristic peaks decreased with the increase of zeolite beta content in hybrid membranes, suggesting that the incorporation of zeolite beta particles can interfere the arrangement of chitosan chains. It was inferred that hydrogen bonds had formed between the –OH groups on the surface of zeolite beta and $–NH_2$ or –OH groups of chitosan, which led to the decrease of intra- and inter-molecular hydrogen bonds of chitosan in CS/Beta hybrid membrane. Additionally, the incorporation of zeolite beta particles can also restrict the mobility of chitosan chain, which was favorable for lowering the methanol permeability of the hybrid membranes [19].

The TGA curves of CS and CS/Beta-2 hybrid membranes were shown in Fig. 5. There were three weight loss stages in the TGA curve of pure CS membrane: the initial weight loss of about 13 wt.% between 40 and 150 °C can be ascribed to the evaporation of adsorbed water; the weight loss of about 69 wt.% between 150 and 240 °C was caused by the degradation of chitosan chains and the weight loss of about 17 wt.% between 240 and 600 °C can be attributed to the decomposition of residual organic groups. For CS/Beta-2 hybrid membranes, the first weight loss stage was similar to that of pure CS membrane and the weight loss between 150 and 240 °C was 10–16 wt.%, which was much lower than that of pure CS membrane. This result indicated that CS/Beta hybrid membranes displayed higher thermal stability than pure CS membrane, which could be ascribed to the hydrogen-bonding interaction between –OH groups on the surface of zeolite beta and –OH or $–NH_2$ groups of chitosan [21]. Furthermore, as the content of zeolite beta increased, the thermal stability of CS/Beta hybrid membranes increased gradually owing to the enhancement of hydrogen bonds and decrease of organic fraction in the membranes.

3.1.3. Water/methanol uptake and IEC

Water and methanol uptake of membranes have an important influence on their performance, such as methanol crossover and proton conduction. Fig. 6 showed the water and methanol uptake of CS and CS/Beta hybrid membranes. It can be observed that both water and methanol uptake decreased with the increase of zeolite beta content in hybrid membranes. This should be attributed to two possible reasons: one is that zeolite beta is more hydrophobic than chitosan; the other is that the addition of zeolite beta rigidifies chitosan chains, resulting in the decrease of their capability to adsorb solvent molecules. At the same zeolite beta content, the water uptake of CS/Beta hybrid membranes was

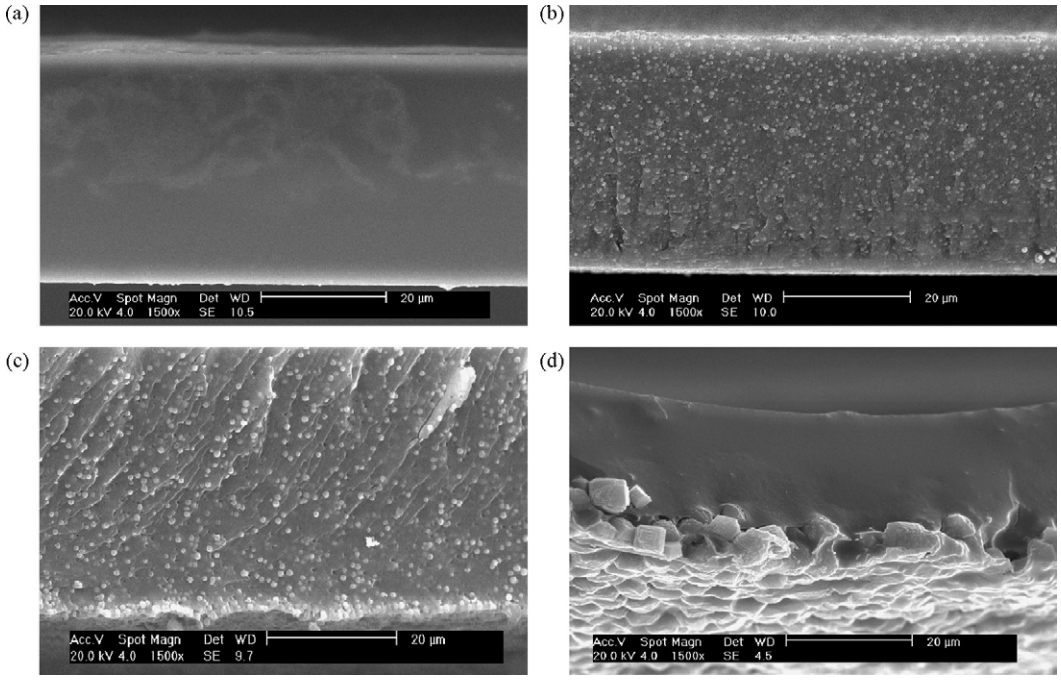

Fig. 3. Cross-section SEM images of CS and CS/Beta hybrid membranes: (a) CS membrane; (b) CS/Beta-1–30%; (c) CS/Beta-2–30% and (d) CS/Beta-3–30%.

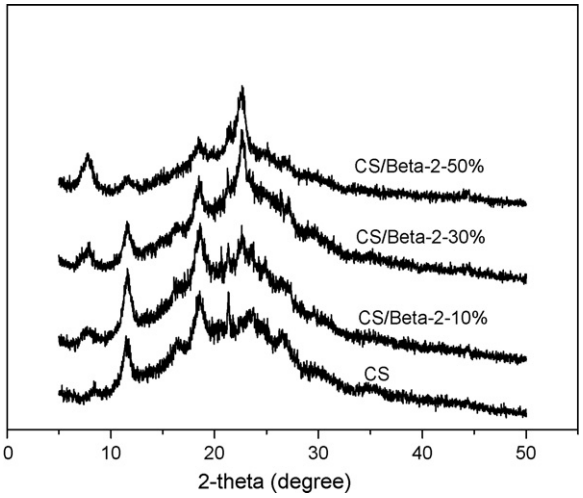

Fig. 4. XRD spectra of CS and CS/Beta hybrid membranes.

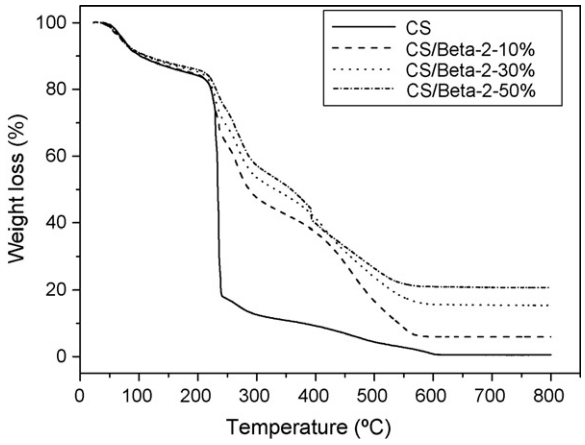

Fig. 5. TGA curves of CS and CS/Beta hybrid membranes.

much higher than the methanol uptake, indicating that these membranes had priority to adsorb water molecules. Moreover, the water uptake of CS/Beta hybrid membranes ordered as follows: CS/Beta-1 > CS/Beta-2 > CS/Beta-3. Beta-1 has smaller size and larger specific surface area than Beta-2 and Beta-3, which makes the CS/Beta-1 membrane adsorb and retain more water molecules. At the same zeolite beta content, the order of methanol uptake was CS/Beta-3 > CS/Beta-1 > CS/Beta-2. Because of the phase separation of zeolite beta and chitosan in CS/Beta-3 membrane, the methanol uptake was close to that of pure CS membrane. Thus, CS/Beta-3 membrane displayed the abnormally high methanol uptake.

IEC provides an indication of ion exchangeable groups present in membrane, which is an indirect value to evaluate the proton conductivity of PEM [30]. As listed in Table 1, the IEC value of pure CS membrane was 0.161 mmol g^{-1}, in agreement with that reported previously [20]. As the content of zeolite beta increased, the IEC values of CS/Beta hybrid membranes showed a decreasing

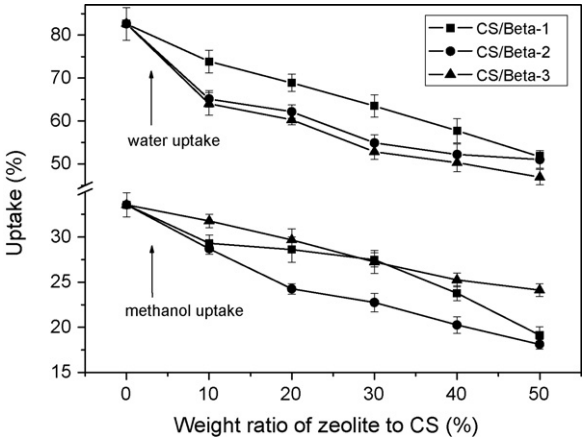

Fig. 6. Water and methanol uptake of CS and CS/Beta hybrid membranes.

Table 1
IEC (mmol g^{-1}) values of CS and CS/zeolite beta hybrid membranes

Membrane	Weight ratio of zeolite to CS (%)					
	0	10	20	30	40	50
CS	0.161					
CS/Beta-1		0.130	0.096	0.082	0.071	0.068
CS/Beta-2		0.115	0.093	0.073	0.068	0.069
CS/Beta-3		0.103	0.114	0.082	0.077	0.065
CS/BetaSO_3H-1		0.129	0.113	0.087	0.086	0.095
CS/BetaSO_3H-2		0.114	0.108	0.096	0.103	0.093
CS/BetaSO_3H-3		0.117	0.110	0.105	0.094	0.090

trend. This can be assigned to the lower ionic conductivity of zeolite beta (10^{-4} S cm^{-1}) [23] than that of chitosan matrix (10^{-3} S cm^{-1}) [31]. Compared with CS/Beta-2 and CS/Beta-3 hybrid membranes, CS/Beta-1 hybrid membranes exhibited slightly higher IEC values. Since Beta-1 had the largest specific surface area among three zeolite samples, more –OH groups were exposed on its surface accordingly, resulting in the highest IEC values of CS/Beta-1 membranes.

3.1.4. Methanol permeability, proton conductivity and selectivity

In the previous study [20], it was found that with the increase of methanol concentration, the methanol permeability of Nafion® 117 membrane showed an increasing trend while the opposite trend was found for CS membrane. Therefore, 2 and 12 mol L^{-1} aqueous solution of methanol were used as feedstocks in this study to investigate different performances of CS/zeolite beta hybrid membranes at low and high methanol concentration, respectively.

The methanol permeability, proton conductivity and selectivity of Nafion® 117, CS and CS/Beta hybrid membranes were listed in Table 2. The methanol permeability of Nafion® 117 membrane was 2.74×10^{-6} and 3.23×10^{-6} cm^2 s^{-1} at methanol concentration of 2 and 12 mol L^{-1}, respectively. Compared with Nafion® 117 membrane, pure CS membrane exhibited lower methanol permeability at both low and high methanol concentration. When zeolite beta particles were introduced into CS membrane, the methanol permeability decreased further. Among three series of CS/Beta hybrid membranes, CS/Beta-2–30% membrane exhibited the lowest methanol permeability of 7.04×10^{-6} and 2.46×10^{-6} cm^2 s^{-1} at methanol concentration of 2 and 12 mol L^{-1}, respectively. The two values were only 25% and 8% of Nafion® 117 membrane, much lower than those reported in our previous study. The incorporated zeolite beta particles can extend the diffusion path length of methanol in the membrane, rigidify the chitosan chains, and compress the volumes among chitosan chains. These reasons caused the decrease in methanol crossover of CS/Beta hybrid membranes.

Table 3
Methanol permeability (P) of CS/zeolite hybrid membranes

Zeolite type	Methanol concentration (mol L^{-1})	P ($\times 10^{-7}$ cm^2 s^{-1})	Reference
Mordenite	12	4.90	[19]
Y[a]	2	9.04	[20]
Y[a]	12	3.90	[20]
A	5	11.18	[21]
13X	5	11.90	[21]
ZSM-5	5	6.24	[21]

[a] Surface modification by MPTMS.

It was noted that most of CS/Beta-2 membranes exhibited lower methanol permeability than CS/Beta-1 and CS/Beta-3 membranes at the same zeolite content. Since Beta-2 particles possessed larger size, they provided longer diffusion path for methanol molecules than Beta-1. Moreover, the methanol molecules won more chance to enter the micropores of larger particles in their diffusion through the membranes. Therefore, the CS membranes filled by Beta-2 with moderate size exhibited the lower methanol permeability. As for CS/Beta-3 membranes, the substantial phase separation between CS and Beta-3 sample constituted the main reason leading to its higher methanol permeability. Even so, their methanol permeability was still much lower than those of pure CS and Nafion® 117 membrane. It was inferred that the inorganic layer composed of Beta-3 particles may play a crucial role in the decrease of methanol permeability.

Compared with other CS/zeolite hybrid membranes reported in the literatures (Table 3), CS/Beta hybrid membranes prepared in this study exhibited much lower methanol permeability. This can be ascribed to the following two possible reasons. On one hand, zeolite beta with high Si/Al ratio was more hydrophobic than

Table 2
Methanol permeability (P), proton conductivity (σ) and selectivity (β) of Nafion® 117, CS and CS/zeolite beta hybrid membranes

Membrane	MC[a] (mol L^{-1})	P ($\times 10^{-7}$ cm^2 s^{-1})					σ ($\times 10^{-2}$ S cm^{-1})					β ($\times 10^4$ S s cm^{-3})				
		10%[b]	20%[b]	30%[b]	40%[b]	50%[b]	10%[b]	20%[b]	30%[b]	40%[b]	50%[b]	10%[b]	20%[b]	30%[b]	40%[b]	50%[b]
CS/Beta-1	2	9.16	7.13	8.96	7.35	7.91	1.53	1.43	1.44	1.34	1.06	1.67	2.82	1.61	1.82	1.34
	12	3.42	2.82	3.45	3.69	3.23						4.47	5.07	4.17	3.63	3.28
CS/Beta-2	2	8.62	8.30	7.04	7.25	7.84	1.49	1.47	1.27	1.22	1.13	1.73	1.77	1.80	1.68	1.44
	12	3.65	3.54	2.46	3.64	3.84						4.08	4.15	5.16	3.35	2.94
CS/Beta-3	2	7.89	7.32	7.27	7.49	8.49	1.36	1.48	1.38	1.15	1.10	1.72	2.02	1.90	1.54	1.30
	12	3.28	2.74	3.65	3.94	4.58						4.15	5.40	3.78	2.92	2.40
CS/BetaSO_3H-1	2	9.19	7.03	6.70	7.72	9.55	1.49	1.47	1.43	1.34	1.19	1.62	2.09	2.09	1.74	1.25
	12	3.68	2.90	2.77	4.26	4.74						4.05	5.07	5.16	3.15	2.51
CS/BetaSO_3H-2	2	7.33	7.13	7.36	8.44	8.99	1.38	1.32	1.43	1.37	1.23	1.88	1.85	1.94	1.62	1.37
	12	4.11	3.70	3.14	4.08	4.58						3.36	3.57	4.55	3.36	2.69
CS/BetaSO_3H-3	2	7.38	6.63	6.35	5.80	7.80	1.32	1.55	1.41	1.34	1.17	1.79	2.34	2.22	2.31	1.50
	12	2.77	2.37	2.07	2.45	3.09						4.77	6.54	6.81	5.47	3.79
CS	2			11.7					1.74					1.49		
	12			5.31										3.28		
Nafion® 117	2			27.4					4.70					1.71		
	12			32.3										1.46		

[a] MC represented methanol concentration.
[b] Value represents weight ration of zeolite to CS.

mordenite, A, X and Y zeolite with low Si/Al ratio. Thus, zeolite beta can preferentially adsorb methanol molecules over water molecules. This can decelerate the transport of methanol molecules in zeolite beta particles, subsequently decrease the methanol permeability of membrane further [21]. On the other hand, self-synthesized zeolite particles had regular morphology and narrow particle size distribution compared with ball-milled zeolite. This can reduce the formation of non-selective voids in the hybrid membranes, more methanol molecules will diffuse through the micropores of zeolite rather than through chitosan–zeolite interface, which is obviously favorable for the methanol rejection.

As listed in Table 2, CS and Nafion® 117 membrane showed proton conductivity of 1.74×10^{-2} and 4.70×10^{-2} S cm^{-1} at 20 ± 1 °C, respectively. They were not consistent with the values reported in the literatures, which can be assigned to different test methods and conditions. Generally, there are two kinds of mechanisms [32] for elucidating proton conduction in the PEM for DMFC: one is Grotthus or "jump" mechanism, which can be idealized as protons passing down the chain of water molecules and ion exchange sites; the other is vehicle mechanism, which assumes that the protons combine with solvent molecules to yield complexes like H_3O^+ or $CH_3OH_2^+$, and then diffuse as a whole across the membrane. It seems that both mechanisms exist in the proton conduction of CS membrane [30]. According to the vehicle mechanism, the amount of water in membrane significantly affects the proton conductivity. In this study, the incorporation of zeolite beta particles into CS membrane significantly reduced the water and methanol uptake, and thus reduced the proton conductivity to a certain extent. The highest water uptake of CS/Beta-1 membranes enabled their highest proton conductivity.

In the membrane separation process such as pervaporation and gas separation, selectivity, a parameter defined as the ratio of permeation flux of two components, was usually used to evaluate the separation efficiency. For DMFC application, a similar parameter could be defined as $\beta = \sigma/P$ to evaluate the selectivity of PEM for proton and methanol, where σ and P described the proton flux and methanol flux, respectively [1]. The expression of β could be deduced according to the Nernst–Plank equation and the Fick's law. The expression of β is an approximate equation, since the electro-osmotic drag presenting in almost all of polymer electrolyte membranes can also influence the methanol transport in membrane besides the concentration gradient [33–35]. However, it was still a useful parameter to evaluate a proton exchange membrane for DMFC, which has been used in many literatures [1,2,11,17,19–21,36]. As listed in Table 2, the selectivity of CS/Beta hybrid membranes basically exhibited the first increasing and then decreasing trend with the increase of zeolite content. This is consistent with the changing trend of methanol permeability of CS/Beta hybrid membranes owing to the unremarkable change of their proton conductivity. Compared with Nafion® 117 membrane, most of hybrid membranes exhibited comparable, even higher selectivity at 2 mol L^{-1} methanol concentration. At 12 mol L^{-1} methanol concentration, all hybrid membranes exhibited much higher selectivity than that of Nafion® 117 membrane. CS/Beta-3–20% showed the highest selectivity of 5.40×10^4 S s cm^{-3}, which was 1.65 and 3.70 times higher than that of pure CS membrane and Nafion® 117 membrane, respectively.

3.2. CS/BetaSO$_3$H hybrid membrane

To improve the compatibility between rigid zeolite beta particles and flexible chitosan in the hybrid membrane, Beta-2 was further sulfonated owing to the lowest methanol permeability of CS/Beta-2 hybrid membranes. Moreover, chitosan membranes filled by sulfonated zeolite beta particles were prepared and their performances were investigated.

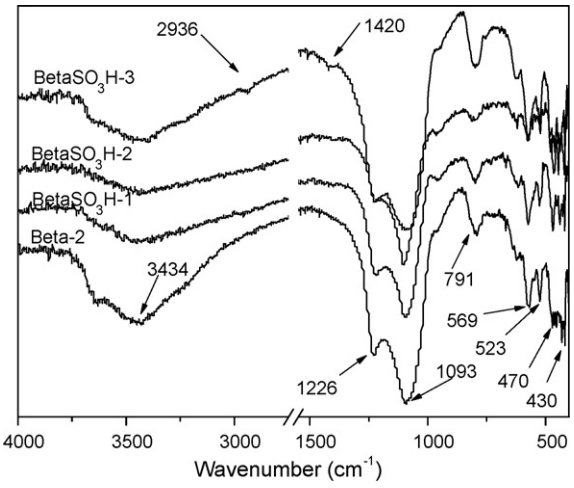

Fig. 7. FT-IR spectra of zeolite beta before and after sulfonation.

3.2.1. Structure of sulfonated zeolite beta

The sulfonated zeolite beta particles were characterized by FT-IR and XPS. The FT-IR spectra of zeolite beta particles before and after sulfonation were shown in Fig. 7. The peaks at 1226 (ν_{as}), 1093 (ν_{as}) and 791 cm^{-1} (ν_s) were assigned to the vibrations of the (Si, Al)O_4 tetrahedral units, which designated as TO_4 in the framework of zeolite beta. The peaks at 430 and 470 cm^{-1} were assigned to pore open and TO bend, respectively. The peaks at 523 and 569 cm^{-1} were assigned to double ring vibrations. All of these peaks belonged to the FT-IR vibrations of zeolite beta, in good agreement with those reported in the literature [37]. After sulfonation, no obvious change in the characteristic peaks (400–1400 cm^{-1}) can be observed, indicating that the chemical framework structure of zeolite beta remained. The distinct peaks of sulfonic acid group (often appeared in 1000–1200 cm^{-1}) could not be discriminated in FT-IR spectra because they were overlapped by the peaks of TO_4. However, the intensity of peak at 3434 cm^{-1} (ν_s), coming from hydroxyl group on the surface of zeolite beta, decreased notably after sulfonation. This can be attributed to the consumption of hydroxyl groups through dehydrating or condensing with sulfonation reagents [20]. In addition, two new peaks at 1420 (ν_b) and 2936 cm^{-1} (ν_s), attributed to the vibration of –CH_2 groups of MPTMS, can be found in the FT-IR spectrum of BetaSO$_3$H-3 sample, suggesting successful modification of zeolite by MPTMS.

To further confirm the occurrence of sulfonation, XPS analysis was conducted. Fig. 8 illustrated the S2p XPS spectra of zeolite beta sulfonated by different reagents. The peaks at binding energy of 168.7 and 163.2 eV were attributed to S^{6+} and S^{2-}, respectively. The peak of S^{6+} should come from –SO_3H group, proving the successful sulfonation on the surface of zeolite beta. The relative content of sulfur was 0.22% and 1.60% for BetaSO$_3$H-1 and BetaSO$_3$H-2, respectively. In the case of BetaSO$_3$H-3 (Fig. 8c), the additional peak of S^{2-} can be attributed to –SH group, which was not completely oxidized by H_2O_2 [20]. The relative content of sulfur on the surface of BetaSO$_3$H-3 sample was 2.29%, of which 1.33% came from –SO_3H group.

3.2.2. Structure of CS/BetaSO$_3$H hybrid membranes

The XRD spectra of CS/BetaSO$_3$H hybrid membranes were presented in Fig. 9. The characteristic peaks of chitosan in CS/BetaSO$_3$H hybrid membranes exhibited much lower intensity than those in CS/Beta hybrid membranes. This indicated that there was strong

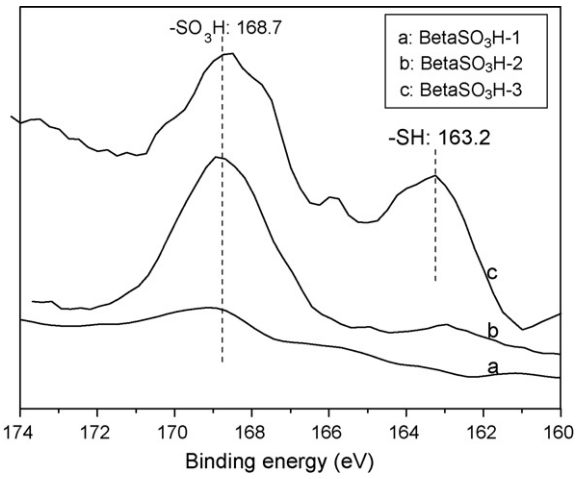

Fig. 8. XPS spectra in S2p core level region of sulfonated zeolite beta.

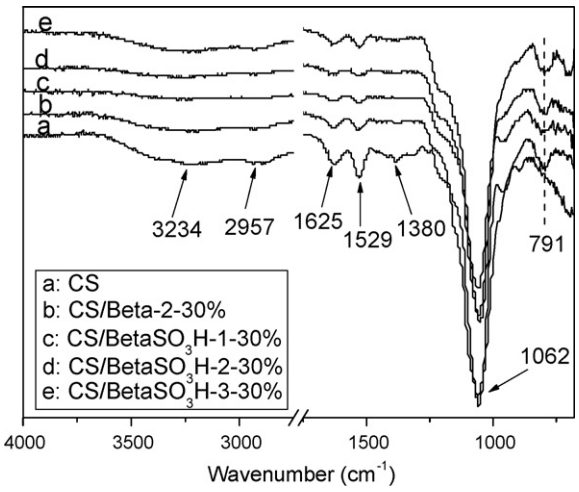

Fig. 10. FT-IR spectra of CS and CS/zeolite beta hybrid membranes.

interaction between chitosan and sulfonated zeolite beta, which came from the ionic interaction between $-SO_3H$ groups on the surface of sulfonated zeolite and $-NH_2$ groups of chitosan. This stronger ionic interaction would destroy the crystal structure of chitosan around zeolite beta particles, and improve the compatibility between rigid zeolite particles and flexible chitosan chains, which was favorable for methanol rejection.

Fig. 10 showed the FT-IR spectra of CS,CS/Beta-2–30% and CS/BetaSO_3H hybrid membranes. From Fig. 10a, it can be seen that the characteristic peaks of chitosan, i.e., the hydroxyl group, amide I and amide II bands, were located at 3234, 1625 and 1529 cm^{-1}, respectively. The peaks at 2957, 1380 and 1062 cm^{-1} were assigned to $-CH_2$ stretching, $-CH_2$ bending and C–O stretching, respectively [38]. The distinct peak at 791 cm^{-1} appeared in the FT-IR spectra of hybrid membranes (Fig. 10b–e) was assigned to TO stretching of zeolite beta. It was noted that the intensity of hydroxyl group, amide I and amide II bands in hybrid membranes obviously decreased compared with those in CS membrane. This was caused by the hydrogen-bonding or ionic interaction between $-NH_2$, –OH groups of chitosan and $-SO_3H$, –OH groups on the surface of zeolite beta.

The TGA curves of CS/BetaSO_3H hybrid membranes were presented in Fig. 11. It can be observed that CS/BetaSO_3H hybrid membranes exhibited similar thermal degradation behaviors as CS/Beta-2–30% membrane. However, the weight losses of three CS/BetaSO_3H-30% membranes in the temperature range of 150–240 °C (13–15 wt.%) was lower than that of CS/Beta-2–30% membrane (16 wt.%). The ionic interaction between $-SO_3H$ groups and $-NH_2$ groups should be responsible for the increased thermal stability. In three kinds of CS/BetaSO_3H hybrid membranes, CS/BetaSO_3H-2–30% and CS/BetaSO_3H-3–30% exhibited a little high thermal stability than CS/BetaSO_3H-1–30%, when the temperature was under 400 °C. This may be attributed to more $-SO_3H$ groups on the surface of zeolite sulfonated by PTMS and MPTMS, leading to the formation of more ionic bonds between zeolite beta and chitosan.

3.2.3. Water/methanol uptake and IEC

Fig. 12 showed the water and methanol uptake of CS/BetaSO_3H hybrid membranes. It can be observed that both water and methanol uptake decreased with the increase of sulfonated zeolite beta content in the hybrid membrane, similar to the results of CS/Beta hybrid membranes. However, both water and methanol uptake of CS/BetaSO_3H hybrid membranes were higher than those of CS/Beta hybrid membranes. In addition, CS/BetaSO_3H-1 hybrid membranes displayed a little higher water and methanol uptake than CS/BetaSO_3H-2 and CS/BetaSO_3H-3 hybrid membranes. The IEC values of CS/BetaSO_3H hybrid membranes were listed in Table 1. Compared with CS/Beta-2 hybrid membranes, all three series of CS/BetaSO_3H hybrid membranes exhibited higher IEC values. These

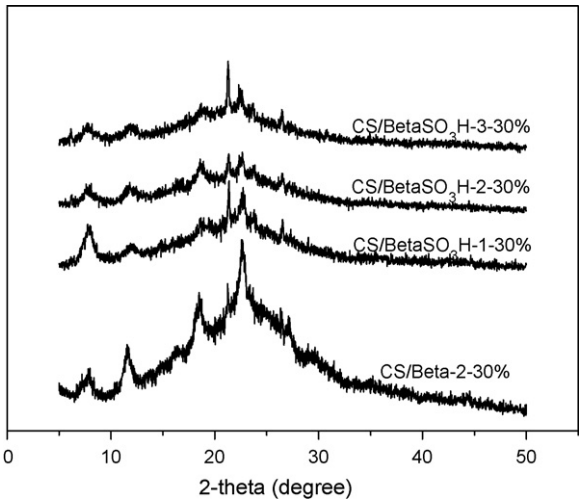

Fig. 9. XRD spectra of CS/Beta-2–30% and CS/BetaSO_3H hybrid membranes.

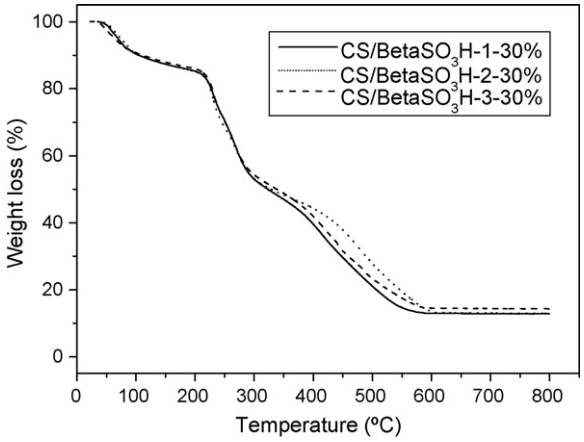

Fig. 11. TGA curves of CS/BetaSO_3H hybrid membranes.

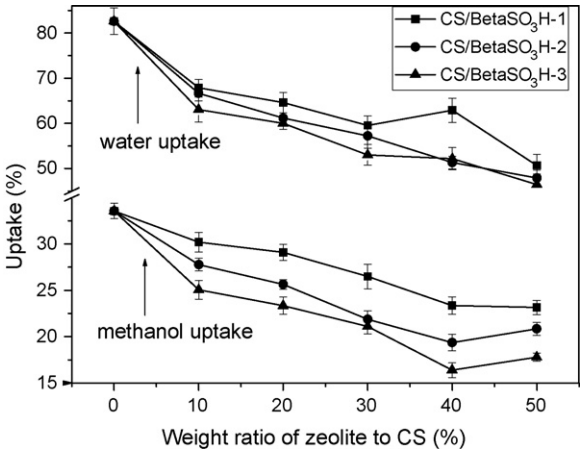

Fig. 12. Water and methanol uptake of CS/BetaSO_3H hybrid membranes.

results suggested that the sulfonation of zeolite beta particles was favorable for the increase of water/methanol uptake and IEC, which correspondingly resulted in the increase of the proton conductivity of these hybrid membranes.

3.2.4. Methanol permeability, proton conductivity and selectivity

The methanol permeability, proton conductivity and selectivity of CS/BetaSO_3H hybrid membranes at methanol concentration of 2 and 12 mol L^{-1} were listed in Table 2. It can be seen that CS/BetaSO_3H-3 hybrid membranes showed the lowest methanol permeability among three series of CS/BetaSO_3H hybrid membranes at both 2 and 12 mol L^{-1} methanol concentration. The lowest methanol permeability of 2.07×10^{-7} cm^2 s^{-1} for CS/BetaSO_3H-3–30% membrane at 12 mol L^{-1} methanol concentration was only about 40% of pure CS membrane and 7% of Nafion® 117 membrane. When comparing with CS/Beta-2 hybrid membrane, CS/BetaSO_3H-3 hybrid membrane exhibited lower methanol permeability at both 2 and 12 mol L^{-1} methanol concentration at the identical zeolite content. It is deduced that the $-SO_3H$ groups on the surface of sulfonated zeolite beta can not only enhance the compatibility between hydrophobic zeolite beta and hydrophilic chitosan matrix, but also decrease the rigidification area between inorganic filler and organic matrix through hydrogen-bonding or ionic interaction with $-NH_2$ or –OH groups of chitosan. Thus, the methanol permeability of CS/BetaSO_3H-3 hybrid membranes further decreased. However, some of CS/BetaSO_3H-1 and CS/BetaSO_3H-2 hybrid membranes displayed higher methanol permeability than that of CS/Beta-2 hybrid membranes at the same zeolite content. This can be attributed to the fact that the content of $-SO_3H$ groups on the surface of BetaSO_3H-1 was quite low (indicated by XPS measurement) and the experimental fluctuation often existed, which resulted in the still relative high methanol permeability. In the case of CS/BetaSO_3H-2 hybrid membrane, compared with propyl group coming from MPTMS, phenyl group coming from PTMS had larger steric hindrance and was not as flexible as propyl group. This was not in favor of the increase of the compatibility between zeolite beta and chitosan matrix, thus led to the relative high methanol permeability.

The proton conductivity of CS/BetaSO_3H hybrid membranes decreased with the increase of sulfonated zeolite beta content in hybrid membranes, similar to the results of CS/Beta-2 hybrid membranes. Furthermore, compared with CS/Beta-2 hybrid membranes, CS/BetaSO_3H hybrid membranes exhibited only a little higher proton conductivity at the same zeolite content. This may be caused by the fact that the $-SO_3H$ groups on the surface of zeolite beta were too short.

Although the increase of proton conductivity was inappreciable, the considerably decreased methanol permeability of CS/BetaSO_3H hybrid membranes resulted in the increase of their selectivity compared with CS/Beta-2 hybrid membranes. Among these membranes, the selectivity of CS/BetaSO_3H-3–30% membrane was 6.81×10^4 S s cm^{-3} at 12 mol L^{-1} methanol concentration, which ranked the highest in the prepared hybrid membranes, and 4.6 times higher than that of Nafion® 117 membrane. The increased selectivity of CS/BetaSO_3H hybrid membranes implied their promising application potential for DMFC.

4. Conclusions

Zeolite beta particles with different sizes were synthesized, and then incorporated into chitosan matrix to prepare CS/zeolite beta hybrid membranes. In the resulting CS/Beta hybrid membranes, CS membranes filled by zeolite beta about 800 nm in size displayed the lowest methanol permeability. This should be attributed to the fact that the moderate size of zeolite beta led to its homogeneous dispersion in CS matrix, and more methanol molecules would diffuse in the micropores of zeolite beta instead of diffuse through the chitosan–zeolite interface. Further sulfonation of zeolite beta particles improved their compatibility with chitosan matrix through increasing the ionic interaction between $-SO_3H$ groups and $-NH_2$ groups. Thereby, most of CS/BetaSO_3H hybrid membranes showed lower methanol permeability and higher selectivity than CS/Beta hybrid membranes. However, their proton conductivity changed only a little, indicating that the vehicle mechanism was dominant in proton conduction. Considering low methanol permeability, moderate proton conductivity, high selectivity, environmental benignity, low cost as well as facile fabrication, CS membranes filled by zeolite beta, especially sulfonated zeolite beta, showed a promising potential for DMFC application.

Acknowledgements

We gratefully acknowledge financial support from the National Nature Science Foundation of China (No: 20776101), the Programme of Introducing Talents of Discipline to Universities (No: B06006) and the Cross-Century Talent Raising Program of Ministry of Education of China. We thank Professor Yuxin Wang for his help in the proton conductivity measurements.

References

[1] B. Libby, W.H. Smyrl, E.L. Cussler, AIChE J. 49 (2003) 991–1001.
[2] C.W. Lin, R. Thangamuthu, P.H. Chang, J. Membr. Sci. 254 (2005) 197–205.
[3] V.D. Noto, R. Gliubizzi, E. Negro, M. Vittadello, G. Pace, Electrochim. Acta 53 (2007) 1618–1627.
[4] R.K. Nagarale, G.S. Gohil, V.K. Shahi, R. Rangarajan, Macromolecules 37 (2004) 10023–10030.
[5] E.A. Aksoy, B. Akata, N. Bac, N. Hasirci, J. Appl. Polym. Sci. 104 (2007) 3378–3387.
[6] Y. Su, Y. Liu, Y. Sun, J. Lai, D. Wang, Y. Cao, B. Liu, M.D. Guiver, J. Membr. Sci. 296 (2007) 21–28.
[7] M.L.D. Vona, Z. Ahmed, S. Bellitto, A. Lenci, E. Traversa, S. Licoccia, J. Membr. Sci. 296 (2007) 156–161.
[8] V.S. Silva, B. Ruffmann, H. Silva, V.B. Silva, A. Mendes, L.M. Madeira, S. Nunes, J. Membr. Sci. 284 (2006) 137–144.
[9] A.S. Aricò, V. Baglio, A.D. Blasi, P. Creti', P.L. Antonucci, V. Antonucci, Solid State Ion. 161 (2003) 251–265.
[10] C.H. Rhee, H.K. Kim, H. Chang, J.S. Lee, Chem. Mater. 17 (2005) 1691–1697.
[11] Z. Cui, C. Liu, T. Lu, W. Xing, J. Power Sources 167 (2007) 94–99.
[12] Z. Chen, B. Holmberg, W. Li, X. Wang, W. Deng, R. Munoz, Y. Yan, Chem. Mater. 18 (2006) 5669–5675.
[13] M.I. Ahmad, S.M.J. Zaidi, S.U. Rahman, Desalination 193 (2006) 387–397.
[14] T. Sancho, J. Soler, M.P. Pina, J. Power Sources 169 (2007) 92–97.
[15] V. Baglio, A.D. Blasi, A.S. Aricò, V. Antonucci, P.L. Antonucci, F. Nannetti, V. Tricoli, Electrochim. Acta 50 (2005) 5181–5188.
[16] X. Li, E.P.L. Roberts, S.M. Holmes, V. Zholobenko, Solid State Ion. 178 (2007) 1248–1255.

[17] S.C. Byun, Y.J. Jeong, J.W. Park, S.D. Kim, H.Y. Ha, W.J. Kim, Solid State Ion. 177 (2006) 3233–3243.
[18] E.N. Gribov, E.V. Parkhomchuk, I.M. Krivobokov, J.A. Darr, A.G. Okunev, J. Membr. Sci. 297 (2007) 1–4.
[19] W. Yuan, H. Wu, B. Zheng, X. Zheng, Z. Jiang, X. Hao, B. Wang, J. Power Sources 172 (2007) 604–612.
[20] H. Wu, B. Zheng, X. Zheng, J. Wang, W. Yuan, Z. Jiang, J. Power Sources 173 (2007) 842–852.
[21] J. Wang, X. Zheng, H. Wu, B. Zheng, Z. Jiang, X. Hao, B. Wang, J. Power Sources 178 (2008) 9–19.
[22] F. Peng, L. Lu, H. Sun, F. Pan, Z. Jiang, Ind. Eng. Chem. Res. 46 (2007) 2544–2549.
[23] B.A. Holmberg, S. Hwang, M.E. Davis, Y. Yan, Micro. Meso. Mater. 80 (2005) 347–356.
[24] P. Mukoma, B.R. Jooste, H.C.M. Vosloo, J. Membr. Sci. 243 (2004) 293–299.
[25] P. Mukoma, B.R. Jooste, H.C.M. Vosloo, J. Power Sources 136 (2004) 16–23.
[26] A. Tolaimate, J. Desbrières, M. Rhazi, A. Alagui, M. Vincendon, P. Vottero, Polymer 41 (2000) 2463–2469.
[27] L. Ding, Y. Zheng, Z. Zhang, Z. Ring, J. Chen, Micro. Meso. Mater. 94 (2006) 1–8.
[28] H. Jon, B. Lu, Y. Oumi, K. Itabashi, T. Sano, Micro. Meso. Mater. 89 (2006) 88–95.
[29] X. Chen, H. Yang, Z. Gu, Z. Shao, J. Appl. Polym. Sci. 79 (2001) 1144–1149.
[30] B. Smitha, S. Sridhar, A.A. Khan, Macromolecules 37 (2004) 2233–2239.
[31] Y. Wan, K.A.M. Creber, B. Peppley, V.T. Bui, J. Appl. Polym. Sci. 89 (2003) 306–317.
[32] K.D. Kreuer, Chem. Mater. 8 (1996) 610–641.
[33] G. Karimi, X. Li, J. Power Sources 140 (2005) 1–11.
[34] V.M. Barragán, C. Ruíz-Bauzá, J.P.G. Villaluenga, B. Seoane, J. Membr. Sci. 236 (2004) 109–120.
[35] X. Ren, T.E. Springer, T.A. Zawodzinski, S. Gottesfeld, J. Electrochem. Soc. 147 (2000) 466–474.
[36] C.W. Lin, Y.F. Huang, A.M. Kannan, J. Power Sources 171 (2007) 340–347.
[37] C.T. Brigden, C.D. Williams, Micro. Meso. Mater. 100 (2007) 118–127.
[38] P. Kanti, K. Srigowri, J. Madhuri, B. Smitha, S. Sridhar, Sep. Purif. Tech. 40 (2004) 259–266.